

Preliminary design and comparative study of thermal control in a nanosatellite through smart variable emissivity surfaces

Proc IMechE Part G:
J Aerospace Engineering
0(0) 1–15
© IMechE 2018
Article reuse guidelines:
sagepub.com/journals-permissions
DOI: 10.1177/0954410018795809
journals.sagepub.com/home/pig



N Athanasopoulos , J Farmasonis and NJ Siakavellas

Abstract

The thermal radiation that is rejected or absorbed into deep space is highly variable. Ultralight smart surfaces with arrays of unit cells can be designed to change their effective emissivity and absorptivity without energy consumption, actuators, and controllers, and can be used for the temperature control of satellites. The smart surfaces work in a similar manner to thermal louvers but they are hingeless, lighter, and their activation depends on their anisotropic mechanical properties and multilayer structure. The generated thermal stresses between layers that have a high mismatch in the coefficient of thermal expansion cause large deformations and rotations within small temperature changes. The arrays of the surface open or close, and transform their geometry as a function of temperature; therefore, coatings of different thermo-optical properties are revealed or concealed, thus creating variable emissivity surfaces. The emissivity and absorptivity curves of the smart surfaces can be entirely designed as a function of temperature. Theoretically, an emissivity change equal to $\Delta\epsilon = 0.8$ can be achieved. The small thermal capacitance renders nanosatellites very susceptible to temperature fluctuations. In this study, different emissivity curves were generated to re-calculate the worst cold and hot cases, and to redesign the thermal control system of a certain nanosatellite. We studied a plethora of design cases based on the energy balance equation in steady state while considering the nanosatellite as one-node geometry. In two ideal designs, the temperature deviation of the nanosatellite in the worst cold and hot cases is limited to $\Delta T = 37^\circ\text{C}$ or 43°C without the use of heaters. Moreover, with a power equal to 0.7W the temperature deviation is limited to $\Delta T = 20^\circ\text{C}$. Consequently, the thermal fatigue is minimized and the energy consumption during the eclipse phase is reduced.

Keywords

Thermal control, variable emissivity surfaces, nanosatellite, smart materials, louvers, radiators

Date received: 19 April 2018; accepted: 30 July 2018

Introduction

Satellites exchange heat with other bodies via thermal radiation, and they control their temperature within the allowable limits using passive and active thermal control systems (TCS). Pressing needs to be addressed are the system complexity, the energy-demand minimization, the reliability, the life span of the satellite, and the incorporation of very small and low-cost satellites in space missions.^{1–6}

Owing to the variable heat inputs, different strategies, devices, and materials are necessary for the thermal control. The most common design approaches for satellite thermal control involve coatings, heavy louvers, large radiators connected to the satellite through heat pipes, heaters, thermostats, heat switches, and controllers.^{7–12} In addition, complex systems have been introduced in order to handle the transient environments and the heat loads using digital turn-down radiators for low lunar orbits.¹³

Moreover, shape memory alloys (SMAs) play a primary role in the development of systems capable of handling the thermal radiation. Reversible thermal panel (RTP) radiators alter their function from a radiator to a solar absorber in order to save power.^{14–17} Similarly, morphable CFRP radiators have been developed and tested.¹⁸ Smaller shape memory structures of a few centimeters allow or prevent the energy exchange with the environment.¹⁹

To boost smaller satellites, engineers in NASA have re-established the classic louver technology by reducing louver dimensions in order to fit them into

Department of Mechanical Engineering & Aeronautics, University of Patras, Patras, Greece

Corresponding author:

N Athanasopoulos, Department of Mechanical Engineering & Aeronautics, University of Patras, Patras, Achaia 26500, Greece.
Email: nikos.athanasop@gmail.com; nathan@mech.upatras.gr

nanosatellites.²⁰ Moreover, extremely complex microelectromechanical devices (MEMs) that incorporate hinges and actuators can actively control the absorption/rejection of thermal radiation for space applications using high-voltage power supplies (microlouvers), and act as variable emissivity surface (VES), thus achieving a fivefold change in their effective thermal emissivity.^{21,22} The performance of the microlouvers has been kept in low levels due to their extensive micro-patterning, complexity, and the use of high-voltage power supplies.

Another promising thermal control solution is the use of electrochromic materials²³ and materials with temperature-dependent thermo-optical properties which can alter their infrared (IR) emissivity from low to high as the temperature increases from 173 K to 375 K²⁴ and from high to low; such a material is VO₂.²⁵

All aforementioned approaches suffer from major drawbacks: the devices are extremely complex and heavyweight; MEMs are heavy, extremely complex, and high cost; certain materials either require power supplies or are incapable of becoming activated at various temperature ranges.

More versatile design strategies are required in order to (a) decrease the temperature fluctuations during the orbit of the satellite and increase the life span, (b) reduce the energy consumption of the electrical heaters.

Ultralight smart surfaces with variable emissivity have been proposed and tested by the present authors.^{26–28} The smart surfaces are able to manipulate thermal radiation passively, without the use of controllers, sensors, and power supplies. The authors proved theoretically and experimentally²⁶ that it is

possible to design the entire emissivity and absorptivity behavior of the smart surface as a function of temperature, and to significantly alter their values ($\Delta\epsilon \approx 0.7–0.8$) using a trilayer material (oriented polyethylene, adhesive, polished aluminum) (Figure 1).

When the unit cells are in the closed position, the effective emissivity is small (Figure 1(d)). As the temperature increases, the unit cells open and the effective emissivity increases owing to the internal high-emissivity coating (Figure 1(d)), thus creating a variable behavior as a function of temperature. Their programmed behavior can be achieved through the prediction of their shape transformation by regulating the view factor of the self-folding unit cells and of the material (coating) that is exposed to the environment, thus creating a surface with variable thermal radiation properties (Figure 1(d)). The temperature-dependent effective thermal properties could follow desired linear or nonlinear profiles and achieve the desired absorptivity / emissivity ratios as a function of temperature.²⁶ These arrays transform their shape via the developed internal stresses, which are due to the anisotropic mechanical properties and the large mismatch of the coefficient of thermal expansion of the multilayer material, and can perform very complex movements with large displacements and rotations. Their behavior is similar to that of “4D biomimetic materials”.²⁹

In this study, our scope is to present a preliminary theoretical study on the thermal control in nanosatellites for the worst cold and hot cases, with and without internal dissipated power by using steady-state energy balance equations and making certain assumptions. A certain nanosatellite (namely COMPASS 1³⁰) was selected in order to redesign its

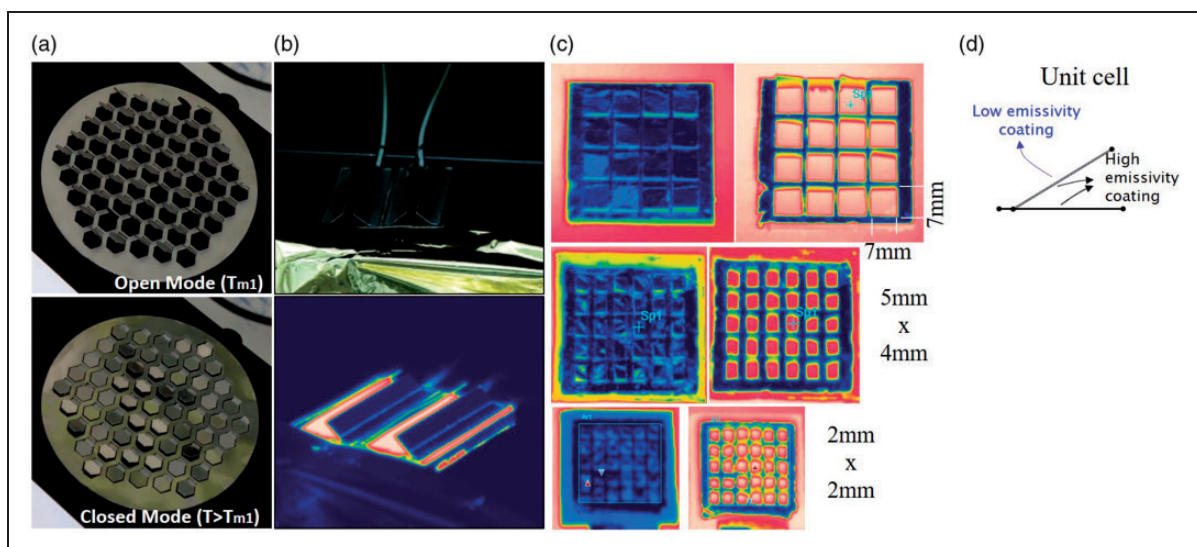


Figure 1. Photographs of different developed smart surfaces using oriented polyethylene, adhesive, and low-emissivity external layers (aluminum or silver).^{26–28} (a) Smart surfaces with hexagonal unit cells, (b) 47 mm × 47 mm smart surfaces with rectangular unit cells,²⁶ (c) thermographic images of the smart surfaces with various unit cell sizes that open and close in less than 40 °C, (d) representation of the unit cell with external low-emissivity coating and internal high-emissivity coating.

thermal control using the emissivity and absorptivity curves of the proposed smart surfaces. We generated different and realistic effective emissivity and absorptivity curves for each side of the nanosatellite using different combinations of smart surfaces and coatings. Our calculations were compared with the calculated cold and hot cases using common paints and materials that were used in COMPASS 1.

Mission, re-design scenarios, and effective material properties

Most of the nanosatellites use passive thermal control strategies, such as a combination of paints and materials of different thermo-optical properties, to find optimized minimum and maximum temperature levels and to reduce the temperature deviation. Most of the designed nanosatellites have demonstrated poor performance in the case of the worst cold case.^{33–41} For this reason, the use of heaters and sensors are necessary for the overcooling protection.

Mission and thermal control of COMPASS-1

The orbit of COMPASS-1 is a circular, synchronous, near-sun low Earth orbit (LEO) at an altitude of 600 km. COMPASS 1 completes one orbital revolution in 96.30 min.^{32–34} The application and the combination of different coatings and materials on the external surfaces of the nanosatellite control the effective emissivity and absorptivity of each side of the nanosatellite.

To increase the minimum temperature of the nanosatellite (worst cold case), it would be ideal to reduce the emissivity of the outer surfaces during the eclipse period. On the other hand, during the hot case, nanosatellites are in a constantly illuminated orbit, and the temperature increases rapidly.

Different combinations of coatings were studied by the COMPASS-1 team for the calculation of the worst hot and cold cases and for the identification of the best coatings' combination. Four different coatings' combinations were used in order to calculate the worst hot and cold cases of this benchmark scenario (scenario A, Figure 2(a)). Sides 1, 2, 3, 5, and 6 were covered 70% by solar cells and 30% by aluminum or 30% by black paint (Figure 2(a)); side 4 carried the antenna and the GPS, and was assumed to consist of 100% black paint or 100% aluminum.³²

Re-design of the thermal control using smart surfaces and calculation of the effective properties

Three different design scenarios (re-design scenarios) namely B, C, and D (Figure 2(b), (c), and (d), respectively), were studied and compared in order to increase the minimum temperature (T_{\min}), decrease the maximum temperature (T_{\max}), and handle the temperature difference of the satellite (ΔT) into certain values. Here, ΔT is the difference of the minimum calculated temperature of the worst cold case and the maximum temperature of the worst hot case $|T_{\max} - T_{\min}|$.

In the design scenario B, sides 1, 2, 3, 5, and 6 are covered 70% by solar cells and 30% by smart surfaces. The smart surfaces open and close in a temperature change $\Delta T_{\text{smart}} = 40^\circ\text{C}$ (Figure 2(b)).

In the design scenario C, sides 1, 2, 3, and 6 are covered 100% by smart surfaces that had been applied over the solar panels, whereas side 4 is covered 100% by smart surfaces. Side 5 is covered 70% by solar cells and 30% by black paint. The smart surfaces open and close in a temperature change $\Delta T_{\text{smart}} = 40^\circ\text{C}$ (Figure 2(c)).

In the design scenario D, sides 1, 2, 3 and 6 are covered 100% by smart surfaces that had been placed

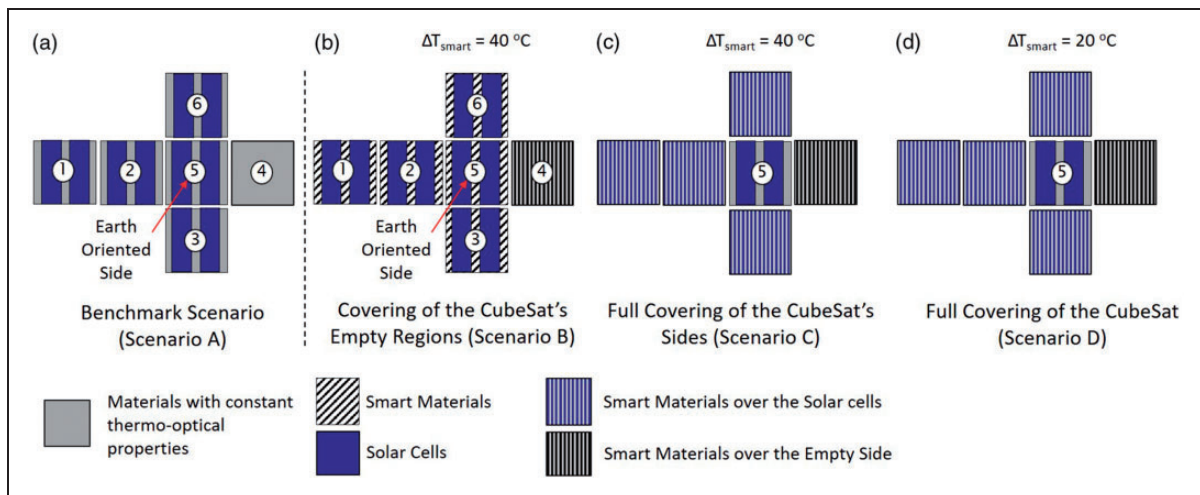


Figure 2. Different design scenarios. (a) Benchmark scenario.³² (b) Scenario B: sides 1, 2, 3, 5, 6 are covered 70% by solar cells and 30% by smart surfaces. (c, d) Scenario C: the solar cells of sides 1, 2, 3, 6 are covered entirely by smart surfaces.

over the solar cells, whereas side 4 is covered 100% by smart surfaces and side 5 is covered 70% by solar cells and 30% by black paint. The smart surfaces open and close in a temperature change $\Delta T_{smart} = 20^\circ\text{C}$ (Figure 2(d)).

In both scenarios (C and D), during the illuminated phase, the unit cells open and the solar cells absorb energy in order to convert it into electrical energy.

Equivalent properties of the sides of the nanosatellite. The emissivity of common materials remains constant with temperature variations and cannot drastically change. However, it is possible to design the entire behavior as a function of temperature, and to significantly alter the thermal emissivity of a surface. The combination of different coatings creates a smart surface with versatile design that can be applied in different satellites and missions. It has been proved by the authors²⁶ that any curve (emissivity or absorptivity) can be generated using the proposed smart surfaces, and can be represented by the bounded curves

$$\epsilon_{eff}(T) = \frac{\epsilon_{min} - \epsilon_{max}}{1 + e^{(T-T_{med})/0.25\Delta T_{smart}}} + \epsilon_{max} \quad (1)$$

$$\alpha_{eff}(T) = \frac{\alpha_{min} - \alpha_{max}}{1 + e^{(T-T_{med})/0.25\Delta T_{smart}}} + \alpha_{max} \quad (2)$$

ϵ_{min} and ϵ_{max} values represent the minimum and maximum effective emissivity values, while α_{min} and α_{max} values represent the minimum and maximum effective absorptivity values. T_0 expresses the temperature at the middle of the curve, whereas ΔT_{smart} represents the temperature span at which the emissivity changes.

Moreover, T_0 along with ΔT_{smart} can be designed to shift to any desired temperature value (Figure 3, red and blue line). The highest effective emissivity value of the smart surfaces is related to the internal coating and the interaction of the unit cells. When the smart surfaces are in the closed state, the radiation leakages were considered to be 1% (the validity of these assumption is related to the technologies that can be used for the manufacturing of the smart surfaces).

The equivalent emissivity of each side of the nanosatellite can be calculated by averaging the thermo-optical properties of the materials in each side

$$\epsilon_{side}(T) = \epsilon_{Mat1} \frac{A_{Mat1}}{A} + \epsilon_{Mat2}(T) \frac{A_{Mat2}}{A} \quad (3)$$

$$\alpha_{side}(T) = a_{Mat1} \frac{A_{Mat1}}{A} + a_{Mat2}(T) \frac{A_{Mat2}}{A} \quad (4)$$

where $\epsilon_{side}(T)$ and $\alpha_{side}(T)$ are the equivalent emissivity and absorptivity of each side, respectively, A_{Mat1} is the area of the solar cells, A_{Mat2} is the area of the smart surface or of a coating with constant thermo-optical properties, A denotes the overall area of each side; ϵ_{Mat1} , a_{Mat1} are the emissivity and the absorptivity of solar cells, respectively, and $\epsilon_{Mat2}(T)$ and $a_{Mat2}(T)$ are the effective emissivity and absorptivity of the smart surfaces, respectively. Consequently, the average emissivity of the five sides that radiate into deep space can be calculated by the following

$$\epsilon'_{IR}(T) = \frac{4\epsilon_{Sides1,2,3,6}(T) + \epsilon_{Side4}(T)}{5} \quad (5)$$

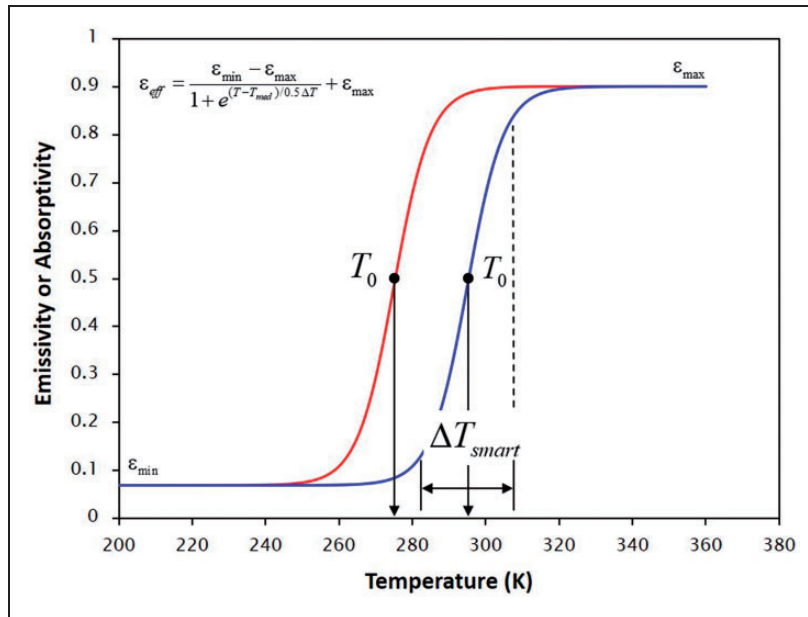


Figure 3. Effective emissivity or absorptivity of smart surfaces. A bounded equation can be generated according to our demands. For example, the curve can be designed to start from $\epsilon_{min} = 0.07$ to $\epsilon_{min} = 0.9$ in $\Delta T_{smart} = 25^\circ\text{C}$ with $T_0 = 20^\circ\text{C}$ (293.15 K), blue curve or $T_0 = 0^\circ\text{C}$ (273.15 K), red curve.

In this study, we assume that one of the sides (side 5) is always directed to earth's surface and the remaining five sides radiate into deep space.³⁰ Moreover, the values of the thermo-optical properties are in the beginning of life (BOL).

Calculation of the worst cold and hot cases

The radiation of the Sun reaching the LEO varies by approximately $\pm 3.5\%$ (\dot{Q}_{sun}). The Earth's albedo accounts for approximately 34% of the incident sunlight that is reflected back to space (\dot{Q}_{Albedo}). In addition, the Earth emits long-wavelength IR radiation with a value of approximately $I_E = 250 \text{ W/m}^2$ (\dot{Q}_{Earth}) and can be modeled as an equivalent black body that emits at 255 K.^{9,10,30-41} Finally, the satellite emits energy to deep space ($\dot{Q}_{Sat-Space}$) and the temperature background for a satellite is approximately equal to 3 K; at the same time, internal dissipated power (\dot{Q}) exists, which is mainly attributed to solar cells, wires, electronic components, or heaters during the eclipse ($\dot{Q} = 1 \text{ W}$). For the preliminary thermal design, we calculated the worst hot and cold cases using the steady-state energy balance equation (6). In our calculations, we considered the nanosatellite as one-node geometry.^{10,30} The terms \dot{Q}_{earth} and $\dot{Q}_{sat \rightarrow earth}$ could be combined into one term, but typical earth IR data is expressed as a heat flux

$$\begin{aligned} \dot{Q}_{sun} + \dot{Q}_{albedo} + \dot{Q}_{earth} + \dot{Q} &= \dot{Q}_{sat \rightarrow space} + \dot{Q}_{sat \rightarrow earth} \Rightarrow \\ &\Rightarrow a_{S_s}(T)I_S A + 0.34a_{S_B}(T)I_S A + a_{IR}(T)I_E A + \dot{Q} \\ &= 5\varepsilon'_{IR}(T)\sigma A(T^4 - T_{space}^4) + \varepsilon_{IR}(T)\sigma A T^4 \end{aligned} \quad (6)$$

where $\varepsilon'_{IR}(T)$ is the average emissivity of the sides of the satellite that reject heat into deep space, $\varepsilon_{IR}(T)$ is the IR emissivity of the Earth-oriented side (Side 5), $a_{S_s}(T)$ is the solar absorptivity, $a_{S_B}(T)$ is the absorptivity of the albedo, .. is the solar absorptivity from the Earth. The solar flux is $I_S = 1370 \text{ W/m}^2$, A is the area of each side of the nanosatellite.

Worst hot and cold cases

In the preliminary design, for the worst hot case, the steady-state temperature can be calculated by the following

$$\begin{aligned} T^4 + \frac{\varepsilon_{IR}(T)\sigma T^4}{5\varepsilon'_{IR}(T)} &= T_{space}^4 + \frac{I_S a_{S_s}(T)}{5\sigma \varepsilon'_{IR}(T)} \\ &+ \frac{I_E \alpha_{IR}(T)}{5\sigma \varepsilon'_{IR}(T)} + \frac{0.34I_S a_{S_B}(T)}{5\sigma \varepsilon'_{IR}(T)} \\ &+ \frac{\dot{Q}}{5\sigma \varepsilon'_{IR}(T)A} \end{aligned} \quad (7)$$

The energy balance equation includes a power dissipation term (\dot{Q}) due to the operation of the solar cells and the electronics. The dissipated power of the nanosatellite is 1 W.³⁰

In the cold case, only the Earth's IR flux exists during the period of the maximum eclipse, without internal dissipation. The temperature of the worst cold case scenario with internal dissipated power (e.g. a heater and electronic component) can be expressed by the following

$$T^4 + \frac{\varepsilon_{IR}(T)T^4}{5\varepsilon'_{IR}(T)} = T_{space}^4 + \frac{I_E \alpha_{IR}(T)}{5\sigma \varepsilon'_{IR}(T)} + \frac{\dot{Q}}{5\varepsilon'_{IR}(T)A\sigma} \quad (8)$$

whereas the temperature of the worst cold case scenario with zero internal energy dissipation, is obtained from equation (8) for $\dot{Q} = 0$.

Calculation of the maximum and the minimum temperature using the regula falsi method

If the material properties are functions of temperature (e.g. $\varepsilon_{IR}(T)$), different numerical iterative methods can be used to extract the solutions. To find the solution of each equation, the regula falsi iterative method was used⁴²

$$T_n = T_{n-1} - \frac{(T_{n-1} - T_{n-2})f(T_{n-1})}{f(T_{n-1}) - f(T_{n-2})}, \quad (9)$$

where $\dot{Q}_{in} - \dot{Q}_{out} = f_{max}(T)$ (equation (7))

$$\begin{aligned} f_{max}(T) &= T^4 + \frac{\varepsilon_{IR}(T)\sigma T^4}{5\sigma \varepsilon'_{IR}(T)} - T_{space}^4 \\ &- \frac{I_S a_{S_s}(T)}{5\sigma \varepsilon'_{IR}(T)} - \frac{I_E \varepsilon_{IR}(T)}{5\sigma \varepsilon'_{IR}(T)} \\ &- \frac{0.34I_S a_{S_B}(T)}{\sigma} - \frac{\dot{Q}}{5\varepsilon'_{IR}(T)A\sigma} \end{aligned} \quad (10)$$

and $\dot{Q}_{in} - \dot{Q}_{out} = f_{min}(T)$ (equation (8))

$$\begin{aligned} f_{min}(T) &= T^4 + \frac{\varepsilon_{IR}(T)\sigma T^4}{5\sigma \varepsilon'_{IR}(T)} - T_{space}^4 \\ &- \frac{I_E \varepsilon_{IR}(T)}{5\sigma \varepsilon'_{IR}(T)} - \frac{\dot{Q}}{5\varepsilon'_{IR}(T)A\sigma} \end{aligned} \quad (11)$$

Assuming the first two values ($T_{n=2}$ and $T_{n=1}$), and after few iterations, the functions $f_{min}(T)$ or $f_{max}(T)$ must converge to zero.

Results and discussion

Scenario A (Benchmark) – Surface finish with constant thermo-optical properties

We conducted benchmark calculations (scenario A) to validate the presented results of COMPASS 1 using

the materials and the combination of materials that had been used by the team (Figure 2(a)).³⁰ The optimal combination of coatings must be selected for the orbit and the design of COMPASS 1. In the benchmark scenario, three different materials were considered, namely: (i) aluminum (Al), (ii) black paint (Bp), and (iii) solar cells (Sc). The emissivity and absorptivity of each material, as well as the equivalent emissivity and absorptivity of the sides, are listed in Table 1.

The following surface finishing combinations were studied, as may be observed in Figure 4 and Table 2:

Case 1. The Earth-oriented side is covered by 70% Sc + 30% Al. Five sides emit energy into deep space; one side is covered by 100% Al and the remaining four sides are covered by 70% Sc + 30% Al. The Sun-oriented side is covered by (a) 70% Sc + 30% Al or (b) 100% Al.

Case 2. The Earth-oriented side is covered by 70% Sc + 30% Al. Five sides emit energy into deep space; one side is covered by 100% Bp and the remaining four sides were covered by 70% Sc + 30% Bp. The Sun-oriented side is covered by (a) 70% Sc + 30% Bp or (b) 100% Bp.

Case 3. The Earth-oriented is covered by 70% Sc + 30% Bp. Five sides emit energy into deep space; one is covered by 100% Al and the remaining four sides are covered by 70% Sc + 30% Al. The Sun-oriented side is covered by (a) 70% Sc + 30% Al or (b) 100% Al.

Case 4. The Earth-oriented side is covered by 70% Sc + 30% Bp. Five sides emit energy into deep space; one side is covered by 100% Bp and the remaining four sides are covered by 70% Sc + 30% Bp. The Sun-oriented side is covered by (a) 70% Sc + 30% Bp or (b) 100% Bp.

The calculated maximum temperature in Case 1, when the Sun-radiated side is covered by 100% Al is equal to $T_{\max} = 36.11^\circ\text{C}$ (309.26 K) and when the

Sun-radiated side is covered by 70% Sc + 30% Al the maximum temperature is equal to $T_{\max} = 8.16^\circ\text{C}$ (281.31 K) (Figure 4(a)).

The worst hot case appears when the Sun-radiated side is covered by 100% Al and the Earth-radiated side is covered by 70% Sc + 30% Bp, Case 3. The calculated temperature in this case is equal to $T_{\max} = 36.82^\circ\text{C}$ (309.97 K) (Figure 4(c)).

Other finishing combinations of materials indicate that the maximum temperature can be reduced more (case 2, Figure 4(b) and case 4, Figure 4(d)). We may conclude that for this mission, the maximum developed temperature cannot cause overheating in any of the components.

In Figure 4, the red bar represents the worst hot case with 1 W heat dissipation, the light blue bar represents the worst cold case with 1 W heat dissipation, the dark blue bar presents the worst cold case without heat dissipation, the black bar represents the temperature difference (ΔT) between the worst hot and cold cases with 1 W heat dissipation and gray bar represents the temperature difference (ΔT) between the worst hot and cold cases without heat dissipation.

The calculated temperatures for the different surface finishing lead the nanosatellite below the cold limits. With zero heat dissipated power, the temperature levels range from $T_{2\min} = -120.14^\circ\text{C}$ (153.01 K) to $T_{2\min} = -90.41^\circ\text{C}$ (182.74 K). With 1 W of heat dissipation, the temperature levels range from $T_{1\min} = -99.83^\circ\text{C}$ (173.32 K) to $T_{1\min} = -72.20^\circ\text{C}$ (200.95 K) (Table 2). The results of the worst cold case with or without internal dissipated power indicate that COMPASS 1 during the eclipse period will be subjected to very low temperature levels. Moreover, the temperature difference ($\Delta T = T_{\max} - T_{2\min}$) of the satellite is significant in all cases and fluctuates between 101.79°C and 138.02°C without internal heat dissipation, while the temperature difference with 1 W internal heat dissipation fluctuates between 87.34°C and 115.29°C . Consequently, alternative passive or active strategies are required, such as thermal blankets, small louvers, or a large heater attached near the batteries.

Scenario B – Application of the variable emissivity surfaces on 30% of the surface of each side

We calculated the worst hot and cold cases using the proposed smart surfaces, which covered only 30% of the surface of each side and 100% of the surface of the empty side (Side 4) of the nanosatellite (Figure 2(b)). The following three different cases were studied (Table 3). For all cases, the Earth-oriented side is covered by 70% Sc + 30% Smart surfaces (Ssf). Five sides emit energy into deep space; one surface is covered by 100% Ssf and the remaining four sides are covered by 70% Sc + 30% Sf. The smart surfaces were designed to open as the temperature increases. Different coating combinations (cases) were

Table 1. Thermo-optical properties that have been used by the Compass-I Team.³⁰

Material	Emissivity (ϵ)	Absorptivity (α)	Side/s
Aluminum	0.080	0.379	
Black paint	0.900	0.970	
Solar cells	0.850	0.920	
Equivalent properties of the nanosatellite's sides			
30% aluminum and 70% solar cells	0.619	0.758	1,2,3,5,6
30% black paint and 70% solar cells	0.865	0.935	1,2,3,5,6
100% aluminum	0.080	0.379	4
100% black paint	0.900	0.970	4

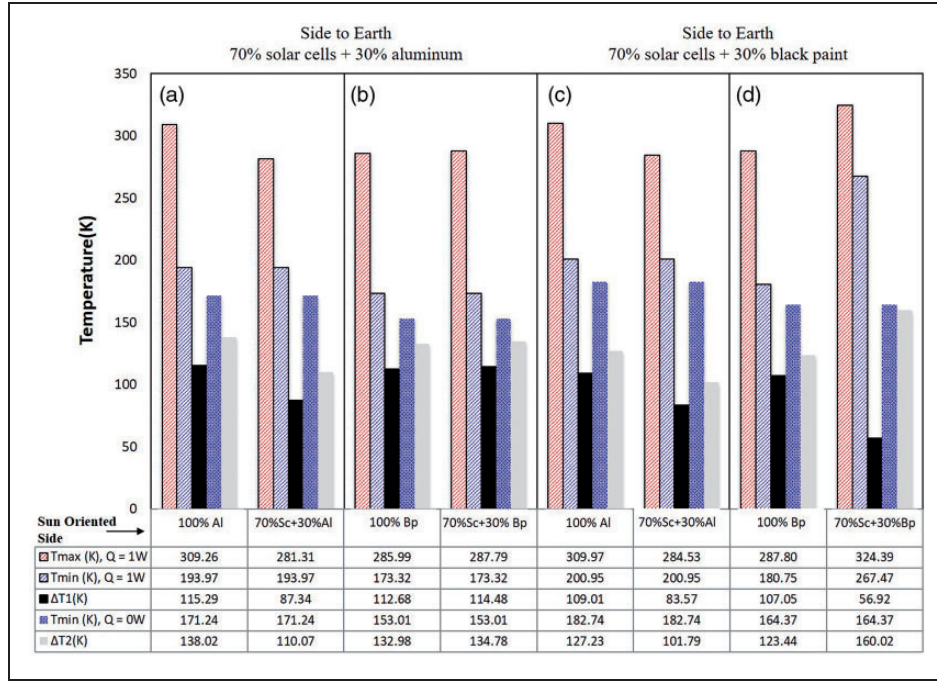


Figure 4. Calculated steady-state temperatures for the worst hot and cold cases for different combinations of materials of the preliminary thermal design of COMPASS 1. (a) Case 1, (b) Case 2, (c) Case 3, (d) Case 4.

considered for the internal and external areas of the smart surface. We assume that the $\epsilon_{IR} = \alpha_{IR}$ equality of the smart surfaces is valid (Figure 5(a)).

Case 1. The first case combines aluminum on the external areas of the smart surface ($\epsilon_{al} = 0.080$, $\alpha_{al} = 0.379$) and black paint on the internal areas of the smart surface ($\epsilon_{bp} = 0.900$, $\alpha_{pb} = 0.970$) (Figure 5(b)).

Case 2. The second case combines silver coating on the external areas of the smart surfaces ($\epsilon_{Pal} = 0.020$, $\alpha_{Pal} = 0.040$) and martin black velvet paint on the internal areas of the smart surface ($\epsilon_{bv} = 0.940$, $\alpha_{bv} = 0.910$) (Figure 5(c)).

Case 3. The third case combines polished aluminum on the external areas of the smart surface ($\epsilon_{Pal} = 0.030$, $\alpha_{Pal} = 0.090$) and white zinc oxide on the internal areas of the smart surface ($\epsilon_w = 0.930$, $\alpha_w = 0.160$) (Figure 5(d)).

The aforementioned bounded equations were used in order to generate the different effective emissivity and absorptivity curves of the smart surfaces (equations (1) and (2)). The equivalent emissivity and absorptivity of the sides as a function of temperature ($\epsilon_{side}(T)$), are summarized in Figure 5(b) and (c) and Appendix 1. The temperature span (ΔT_{smart}) was set to 40°C , and $T_0 = -8.15^\circ\text{C}$ (265 K) for all cases.

The solid lines of Figure 5(b) to (d) represent the equivalent absorptivity and the dashed lines represent the equivalent emissivity of the sides. The red lines represent the sides with the solar cells, the blue lines represent the side that is oriented to the Earth, and the

black lines represent the 100% smart surface side of the nanosatellite.

Because the smart surfaces have been applied to only 30% of the surface of each side of the nanosatellite, the values of the equivalent thermo-optical properties of the sides 1, 2, 3, 5, 6 changed only slightly (e.g. $\Delta\epsilon \approx 0.6 - 0.86$, Figure 5(b)).

The results from the hot case calculations yielded the following results: when the Sun-radiated side is covered by 30% Smart surface + 70% Sc the maximum temperature of the nanosatellite is equal to $T_{max} = 13.11^\circ\text{C}$ (286.27 K) and when the Sun-radiated side is covered by 100% smart surface the maximum temperature is equal to $T_{max} = 14.62^\circ\text{C}$ (287.77 K) (Figure 5(a)). Table 3 presents all the calculated temperature values for various combinations of smart surfaces.

If we compare the second smart surface, the maximum temperatures are equal to $T_{max} = 9.73^\circ\text{C}$ (282.88 K) and $T_{max} = 8.32^\circ\text{C}$ (281.47 K). The other smart surfaces lead to even smaller temperatures e.g. the white zinc oxide lead to very low maximum temperatures ($< 0^\circ\text{C}$). Table 3 presents all the calculated minimum and maximum temperatures for the five different smart surfaces.

We may conclude that if we use the smart surfaces in this mission, the maximum developed temperature would be in excellent levels. On the contrary, once again the cold-case predictions yielded very low temperature levels $T_{min} \approx -72.62^\circ\text{C}$ (200.53 K) to $\approx -70.31^\circ\text{C}$ (202.84 K) with 1 W of internal heat dissipation and $T_{min} \approx -88.54^\circ\text{C}$ (184.60 K) to $\approx -90.90^\circ\text{C}$ (182.25 K) without internal heat dissipation.

Table 2. Calculated hot and cold worst cases of the benchmark design with and without internal dissipated power.

Side		1	2	3	4	6
	30% Al + 70% Sc	30% Al + 70% Sc	30% Al + 70% Sc	100% Al	30% Al + 70% Sc	
	Oriented side to earth (5)					
	Side (5): 70% Sc – 30% Al	T_{max} $Q=1\text{ W}$	T_{min} $Q=1\text{ W}$	T_{min} $Q=0\text{ W}$	$\Delta T1$	$\Delta T2$
Case 1	•	281.31	193.97	171.24	87.34	110.07
	•	309.26	193.97	171.24	115.29	138.02
	30% Black + 70% Sc					
	Oriented side to earth (5)					
	Side (5): 70% Sc – 30% Al	T_{max} $Q=1\text{ W}$	T_{min} $Q=1\text{ W}$	T_{min} $Q=0\text{ W}$	$\Delta T1$	$\Delta T2$
Case 2	•	287.79	173.32	153.01	114.48	134.78
	•	285.99	173.32	153.01	112.68	132.98
	30% Black + 70% Sc					
	Oriented side to earth (5)					
	Side (5): 70% Sc – 30% Black	T_{max} $Q=1\text{ W}$	T_{min} $Q=1\text{ W}$	T_{min} $Q=0\text{ W}$	$\Delta T1$	$\Delta T2$
Case 3	•	284.53	200.95	182.74	83.57	101.79
	•	309.97	200.95	182.74	109.01	127.23
	30% Black + 70% Sc					
	Oriented side to earth (5)					
	Side (5): 70% Sc – 30% Black	T_{max} $Q=1\text{ W}$	T_{min} $Q=1\text{ W}$	T_{min} $Q=0\text{ W}$	$\Delta T1$	$\Delta T2$
Case 4	•	289.48	180.75	164.37	108.73	125.12
	•	287.80	180.75	164.37	107.05	123.44

○ Sun-oriented side; ● Deep-space-oriented side.

Table 3. Calculated worst hot and cold cases of the second design scenario (scenario B), with and without internal dissipated power.

Side		With electrical dissipation ($Q=1\text{ W}$)			No electrical dissipation ($Q=0\text{ W}$)		
Side		T_{max}	T_{min}	$\Delta T1$	T_{max}	T_{min}	$\Delta T2$
1	2	3	4	6	Oriented side to earth (5)		
	30% Smart + 70% Sc	30% Smart + 70% Sc	100% Smart	30% Smart + 70% Sc			
Case 1	Black + Al	•	○	•	286.27	200.68	85.59
	•	•	•	•	287.77	200.68	87.10
Case 2	Martin black velvet paint + Silver	•	○	•	282.88	202.84	80.04
	•	•	•	•	281.47	202.84	78.63
Case 3	White zinc oxide + Aluminum polished	•	○	•	273.66	202.51	71.15
	•	•	•	•	250.26	202.51	47.75

○ Sun-oriented side; ● Deep-space-oriented sides.

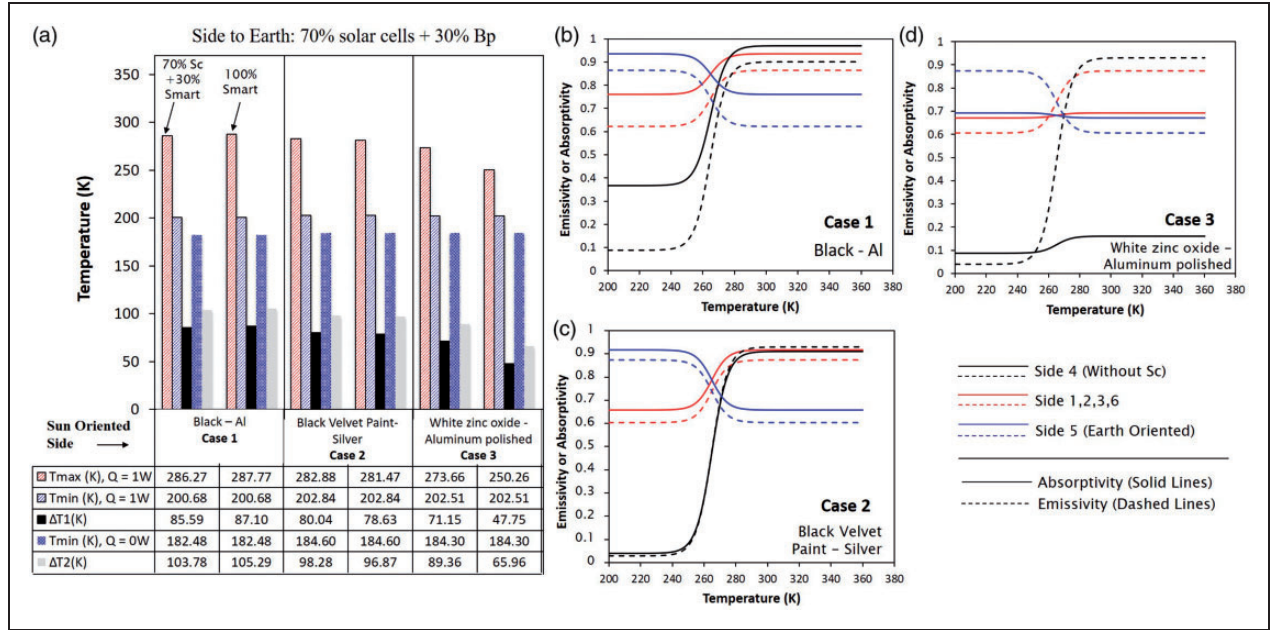


Figure 5. (a) Calculated steady-state temperatures for the worst cases for different combinations of smart surfaces. (b, c, d) Equivalent thermo-optical properties as a function of temperature for cases 1, 2, 3.

In any case, the temperature values for the worst cold case rose while the maximum temperature decreased or remained at the same levels. However, this value is not a sufficient improvement for the overall temperature behavior of the satellite. Owing to these low temperature values, a heater would potentially be needed. Despite the fact that the temperature difference of the satellite ($\Delta T = T_{\max} - T_{\min}$) decreased, the 30% of the area that was occupied by smart surfaces was not sufficient to drastically change the minimum temperature.

Scenario C – Application of the variable effective emissivity surfaces on the entire area of the sides of the nanosatellite

To increase the minimum temperature, we applied the smart surfaces over the solar cells; 90% of the area of the side can open, thus allowing the solar cells to absorb energy. When the nanosatellite is in the eclipse period, the unit cells are in a closed state and the effective emissivity of the sides decreases drastically. In this case, when the nanosatellite would exit the eclipse period, the smart surfaces would open their unit cells, thus allowing the solar cells to absorb light. It becomes obvious that the energy absorbed from the solar cells that is converted to electrical energy will be reduced. This is a matter of redesigning the electrical consumption, which will not be addressed in this study.

We calculated and examined the worst hot and cold cases using the proposed smart surfaces that covered a 100% of the nanosatellite sides (1, 2, 3, 4, 6). The Earth-oriented side was covered by 70% Sc + 30% Bp. The equivalent emissivity and

absorptivity as a function of temperature of the sides are listed in Figure 6(b) to (d). The temperature range (ΔT_{smart}) was set to 40 °C. We observe that the equivalent thermo-optical properties of the sides drastically change their emissivity (e.g. $\Delta\epsilon = 0.1 - 0.9$).

Case 1. The first case combines aluminum on the external areas of the smart surface ($\epsilon_{al} = 0.080$, $\alpha_{al} = 0.379$) and black paint on the internal areas of the smart surface ($\epsilon_{bp} = 0.900$, $\alpha_{pb} = 0.970$). The temperature at the middle of the curve is $T_0 = 0$ °C (273.15 K) (Figure 5(b)).

Case 2. The second case combines silver coating on the external areas of the smart surfaces ($\epsilon_{Pal} = 0.020$, $\alpha_{Pal} = 0.040$) and martin black velvet paint on the internal areas of the smart surface ($\epsilon_{bv} = 0.940$, $\alpha_{bv} = 0.910$). The temperature at the middle of the curve $T_0 = 11.85$ °C (285 K) (Figure 5(c)).

Case 3. The third case combines polished aluminum on the external areas of the smart surface ($\epsilon_{Pal} = 0.030$, $\alpha_{Pal} = 0.090$) and white zinc oxide on the internal areas of the smart surface ($\epsilon_w = 0.930$, $\alpha_w = 0.160$). The temperature at the middle of the curve $T_0 = 11.85$ °C (285 K) (Figure 5(d)).

The results from the hot-case calculations yield the following results (Table 4). Particularly, the maximum temperature of the second case is equal to $T_{\max} = 20.64$ °C (293.79 K), while in the fourth case the maximum temperature is equal to $T_{\max} = 11.92$ °C (285.07 K). The temperature deviation of the benchmark scenario for a maximum temperature near 20 °C (293.15 K) was $\Delta T_{\text{satellite}} = 125$ °C (case 4 of the benchmark scenario) while the temperature deviation of the second and fourth case of scenario

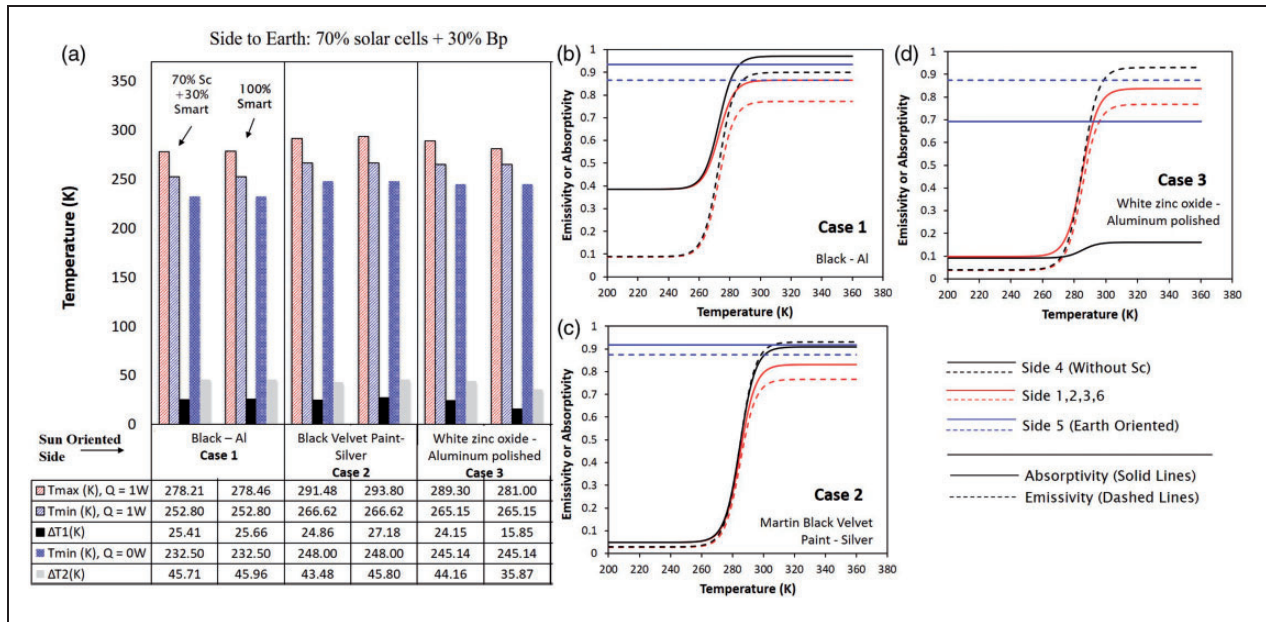


Figure 6. (a) Calculated steady-state temperatures for the worst cases for different combinations of smart surfaces. (b, c, d) Equivalent thermo-optical properties as a function of temperature for cases 1, 2, 3.

Table 4. Calculated worst hot and cold cases of the third design scenario (scenario C), with and without internal dissipated power.

Side	With electrical dissipation (Q̇ = 1 W)					No electrical dissipation (Q̇ = 0 W)				
	1	2	3	4	6	Side 5: Oriented side to earth				
Smart material	100% Smart over the Sc	100% Smart over the Sc	100% Smart over the Sc	100% Smart	100% Smart over the Sc	30% Bp + 70% Sc				
	T _{max}	T _{1min}	ΔT ₁	T _{2min}	ΔT ₂					
Case 1 Black + Al	•	○	•	•	•	278.21	252.80	25.41	232.50	45.71
	•	•	•	○	•	278.46	252.80	25.66	232.50	45.96
Case 2 Martin black velvet paint + Silver	•	○	•	•	•	291.48	266.62	24.86	248.00	43.48
	•	•	•	○	•	293.80	266.62	27.18	248.00	45.80
Case 3 White zinc oxide + Aluminum polished	•	○	•	•	•	289.30	265.15	24.15	245.14	44.16
	•	•	•	○	•	281.00	265.15	15.85	245.14	35.87

○ Sun-oriented side; • Deep-space-oriented side.

C is 45 °C and 37 °C, respectively without internal heat dissipation (Table 4). In Case 2, the maximum temperatures ranges between 5.06 °C (278.21 K) and 5.31 °C (278.46 K) (Figure 7(b)). For the worst cold case without internal energy dissipation, the minimum temperatures range between -40.65 °C (232.15 K) and -25.15 °C (248.15 K). With internal heat dissipation the minimum temperature ranges between -6.53 °C (266.65 K) and -20.35 °C (253.15 K).

We may conclude that this drastic change of the equivalent emissivity of the nanosatellite’s external areas allows the nanosatellite to be operational because the maximum and minimum developed temperatures are between the allowable temperature limits of the electronics and near the lower

temperature limits of the LiPo batteries.³⁴ As a consequence, the power of heaters is minimized. The weight addition in this design scenario will be 16.5 g.

Scenario D – Application of highly sensitive variable smart emissivity surfaces on the entire area of the sides of the nanosatellite

At this point, we would like to present two improved smart surfaces’ design and compare them with the benchmark scenario as function of the internal dissipated heat power during the eclipse. The aforementioned bounded equations were used with a smaller temperature operational range (ΔT_{smart} = 20 °C). This means that the smart surfaces that have been

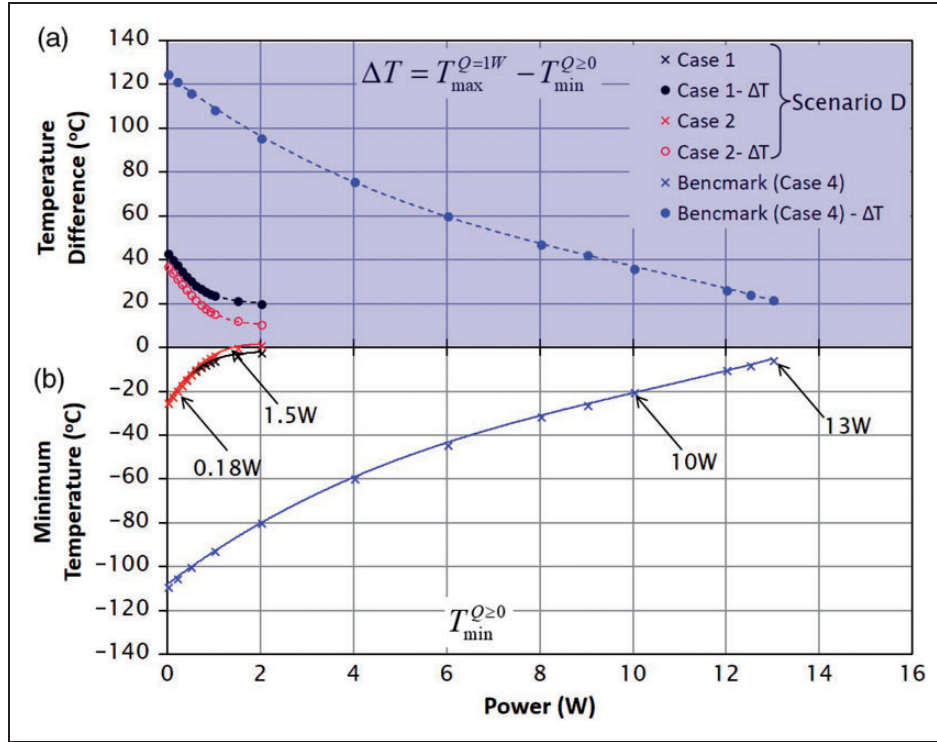


Figure 7. Calculated steady-state temperatures and temperature difference as a function of internal dissipated power for the worst cold case of the optimized smart surfaces (cases 1 and 2) and the benchmark case 4. (a) Temperature difference; (b) calculated worst cold case.

Table 5. Calculated worst hot and cold cases of the fourth design scenario (scenario D), with and without internal dissipated power.

		Side					With electrical dissipation ($\dot{Q} = 1 \text{ W}$)		No electrical dissipation ($\dot{Q} = 0 \text{ W}$)		
		1	2	3	4	6	Side 5: Oriented side to earth				
Smart material		100% Smart over the Sc	100% Smart over the Sc	100% Smart over the Sc	100% Smart	100% Smart over the Sc	30% Bp + 70% Sc T_{\max}	$T_{1_{\min}}$	$\Delta T1$	$T2_{\min}$	$\Delta T2$
Case 1	Martin black velvet paint + Silver	●	○	●	●	●	287.65	267.42	20.23	248.14	39.51
	White	●	○	●	●	●	291.46	267.42	24.03	248.14	43.32
Case 2	White	●	○	●	●	●	285.48	269.82	15.66	248.14	37.33
	zinc oxide + Silver	●	●	●	○	●	278.89	269.82	9.07	248.14	30.75

○ Sun-oriented side; ● Deep-space-oriented side.

applied over the solar cells are more sensitive and open or close into 20°C .

Case 1. The first case combines silver coating on the external areas of the smart surfaces ($\epsilon_{Pal} = 0.020$, $\alpha_{Pal} = 0.040$) and martin black velvet paint on the internal areas of the smart surface ($\epsilon_{bv} = 0.940$, $\alpha_{bv} = 0.910$). The temperature at the middle of the emissivity curve is $T_0 = 3.85^\circ\text{C}$ (277 K) (Figure 7(b)).

Case 2. The second case combines silver coating ($\epsilon_s = 0.020$, $\alpha_s = 0.040$) on the external areas of the smart surface and white zinc oxide on the internal areas of the smart surface ($\epsilon_w = 0.930$, $\alpha_w = 0.160$). The temperature at the middle of

the emissivity curve is $T_0 = 7.85^\circ\text{C}$ (281 K) (Figure 7(d)) (Table 5).

The first goal is to keep in any circumstances the maximum temperature of the nanosatellite below $T_{\max} < 20^\circ\text{C}$ (293.15 K). The second and most critical goal is to increase drastically the minimum temperature in order to minimize or avoid using the energy of the batteries. The maximum calculated temperatures are $T_{\max} = 18.31^\circ\text{C}$ (291.46 K) and 12.33°C (285.48 K), respectively, while the minimum temperature is $T2_{\max} = -25.01^\circ\text{C}$ (248.14 K) (Table 5).

If we set the lower allowable temperature limit equal to $T_{\min} \approx -20^\circ\text{C}$ (293.15 K), we observe that

the power of heaters that will be required to achieve the minimum set temperature is 0.18 W (cases 1 and 2 of scenario D). In contrast, the required power for achieving the $T_{\min} \approx -20^{\circ}\text{C}$ (293.15 K) at steady state using the best benchmark design scenario (case 4) is 10 W. In the case where the lower limit of the satellite is equal to $T_{\min} = 0^{\circ}\text{C}$ (273.15 K), the required power of the best benchmark scenario is more than 13 W while the power of the first case and second case of scenario D is 3 W (case 1) and 1.5 W (Case 2), respectively (Figure 7). The temperature difference $\Delta T_{\text{satellite}} = T_{\max}^{Q=1W} - T_{\min}^{Q \geq 0}$ between the worst hot and cold case of scenario D will be limited to 18.45 °C (291.60 K), case 1 and 12.43 °C (285.58 K), case 2.

Figure 7 presents the calculated lower temperature (T_{\min}) of the satellite and the temperature difference ($\Delta T_{\text{satellite}}$) as a function of the internal heat dissipation for the (a) fourth case of the benchmark scenario (blue lines), (b) first case of scenario D (black lines), and (c) second case of scenario D (red lines). The power during the eclipse period is required in order to regulate the temperature of the satellite between the allowable limits for the one-mode model.

In the first case of the current scenario (scenario D), the power of the heater can be reduced by 98.2% in order to regulate the temperature of the satellite between -20°C (253.15 K) and 18.31°C (291.46 K), or can be reduced by 78.6% in order to regulate the temperature of the satellite between 0°C (273.15 K) and 18.31°C (291.46 K). Similarly, in the second case of the current scenario (scenario D), the power of the heater can be reduced by 98.3% in order to regulate the temperature of the satellite between -20°C (253.15 K) and 11.85°C (285 K), or can be reduced by 89.3% in order to regulate the temperature of the satellite between 0°C (293.15 K) and 11.85°C (285 K). In this case, the smart surface will not entirely open. At this point, it is useful to dictate that the calculated power is high due to the steady-state energy balance calculations. The energy balance equations that have been used take into consideration the steady-state conditions of the nanosatellite and the satellite are considered as one-node geometry. The geometrical characteristics and the internal architecture of the nanosatellite (3D modeling) have not been considered in this study. Therefore, the thermal conduction between the different parts has been eliminated. Usually, this amount of power is not required due the short eclipse period of the nanosatellite and the internal insulative materials that are used for the overcooling protection of the batteries.

Conclusions

A plethora of combinations using the developed smart surfaces was studied in order to calculate the minimum and maximum developed temperature of the worst cold case. The minimum temperature of the

nanosatellite increased drastically in the worst cold case, whereas the maximum developed temperature of the worst hot case remained at the same levels. Because the smart surfaces are located at the external areas of the nanosatellite, the temperature of the entire structure and subsystems will be slightly deviated during the orbit. The temperature difference (difference between the worst hot and cold cases) is decreased, and as a consequence, the thermal fatigue of the overall structure—particularly the thermal fatigue at the joints and adhesives—would decrease drastically. The thermal fatigue of the structural parts, the electronics, and the solar cells practically will be eliminated. According to the mission and the energy requirements of the nanosatellite, a smaller battery may be used for the operation of the electronics in the eclipse. The reduction of the power of heater may also have positive impacts on the area of the solar cells because the batteries will be not charged for the eclipse phase. Regardless of the fact that the power of heater can be minimized or eliminated together with the sensors, cabling, etc., the advantages of the smart surfaces will be present on the overall structure and the materials selection. Moreover, we strongly believe that the transient calculations will reveal much better results and the calculated power will be decreased or eliminated. Higher impact is expected in 2U, 3U, or 6U nanosatellites and microsatellites, as well as in nanosatellites with deployable solar cells, because of the larger external areas.

The fact that we do not use an automatic control system that reacts in order to control the temperature of the satellite leads to the conclusion that the calculations of the behavior of the smart surface must be very accurate. Moreover, the effective emissivity of the smart surfaces is a directional-dependent parameter and must be integrated in future calculations in order to acquire more detailed results.

The degradation of the multilayer material due to UV radiation and the atomic oxygen can be reduced drastically through the incorporation of an extra very thin layer of coated aluminum without altering significantly the performance of the smart surfaces.


Declaration of Conflicting Interests

The author(s) declared no potential conflicts of interest with respect to the research, authorship, and/or publication of this article.

Funding

The author(s) disclosed receipt of the following financial support for the research, authorship, and/or publication of this article: This research was conducted through the IKY scholarships program, and is co-financed by the European Union (European Social Fund (ESF)) and the Greek national funds through the action entitled “Reinforcement of Postdoctoral Researchers” of the National Strategic Reference Framework (NSRF), 2014–2020.

ORCID iD

N Athanasopoulos  <http://orcid.org/0000-0001-6929-3057>

References

- Macdonald M and Badescu V. *The international handbook of space technology*. Heidelberg-New York-Dordrecht-London: Springer-Praxis Publishing, 2014.
- NASA Technology Roadmaps. *NASA Space Technology Roadmaps & Priorities*. Washington: National Academies Press, 2012.
- Baturkin V. Micro-satellites thermal control – Concepts and component. *Acta Astronaut* 2005; 56: 161–170.
- Mission Design Division Staff. *Small spacecraft technology state of the art*. California: Ames Research Center, NASA/TP–2014–216648/REV1, 2014.
- Shea HR. MEMS for pico- to micro-satellites. In: *Photonics West 2009, MOEMS and Miniaturized Systems VIII*, San Jose, CA, USA, 2009.
- Crisp NH, Smith K and Hollingsworth P. Launch and deployment of distributed small satellite systems. *Acta Astronaut* 2015; 114: 65–78.
- Gilmore DG. *Spacecraft thermal control handbook volume I: Fundamental technologies*. El Segundo, CA: The Aerospace Press, 2002.
- Fortescue P, Swinerd G and Stark J. *Spacecraft systems engineering*. 4th ed. West Sussex, UK: John Wiley & Sons, 2011.
- Plamondon J. Analysis of movable louvers for temperature control. *J Spacecraft* 1964; 1: 492–497.
- Furukawa M. Analytical studies on design optimization of movable louvers for space use. *J Spacecraft* 1979; 16: 412–425.
- Arslanturk C. Optimization of space radiators with step fins. *Proc IMechE, Part G: J Aerospace Engineering* 2009; 224: 911–917.
- Arslanturk C. Optimization of space radiators accounting for variable thermal conductivity and base-to-fin radiation interaction. *Proc IMechE, Part G: J Aerospace Engineering* 2016; 232: 121–130.
- Miller JR, Gajanana CB, Ganapathi GB, et al. Design and modeling of a radiator with digital turn-down capability under variable heat rejection requirements. In: *41st international conference on environmental systems*, Portland, OR, USA, 2011.
- Nagano H, Ohnishi A, Nagasaka Y, et al. Study on a reversible thermal panel for spacecraft (detailed design based on parametric studies and experimental verification). *Heat Transfer—Asian Res* 2006; 35: 464–481.
- Nagano H, Ohnishi A, Nagasaka Y, et al. A reversible thermal panel for spacecraft thermal control (evaluation of effectiveness and reliability of new autonomous thermal control device). *Heat Transfer—Asian Res* 2005; 34: 350–367.
- Nagano H, Ohnishi A and Nagasaka Y. Development of a lightweight deployable/stowable radiator for interplanetary exploration. *Appl Therm Eng* 2011; 31: 3322–3331.
- Nagano H and Nagasaka Y. Simple deployable radiator with autonomous. *J Thermophys Heat Transfer* 2006; 20: 856–864.
- Cognata TJ, Hardtl D, Sheth R, et al. A morphing radiator for high-turn-down thermal control of crewed space exploration vehicles. In: *23rd AIAA/AHS adaptive structures conference*, Kissimmee, USA, 2015.
- Matovic L, Vujanic A and Reichenberger K. Variable emissivity surfaces for micro and nanosatellites. In: *CANEUS 2006*, Toulouse, France, 2006, pp.1–6.
- Willingham AL. Cubesat form factor thermal control louvers. Patent_US20170088294A1, USA, 2015.
- Cao S, Xuekang C, Wu G, et al. Variable emissivity surfaces for micro and nano-satellites. *Phys Procedia* 2011; 18: 91–94.
- Darrin AG, Osiander R, Champion J, et al. Variable emissivity through MEMS technology. In: *Thermal and thermomechanical phenomena in electronic systems*, Las Vegas NV, USA, 2000, paper no. 6754928.
- Paris A, Anderson K, Zay B, et al. Electrochromic radiators for microspacecraft thermal control. In: *19th annual AIAA/USU conference on small satellites*, Logan UT, USA, 2005.
- Tachikawa S and Ohnishi A. Development of a variable emittance radiator based on a perovskite manganese oxide. *J Thermophys Heat Transfer* 2003; 17: 1–5.
- Kats M, Blanchard R, Zhang S, et al. Vanadium dioxide as a natural disordered metamaterial: Perfect thermal emission and large broadband negative differential thermal emittance. *Phys Rev X* 2014; 3: 1–7.
- Athanasopoulos N and Siakavellas NJ. Smart patterned surfaces with programmable thermal emissivity and their design through combinatorial strategies. *Sci Rep* 2017; 7: 12908.
- Athanasopoulos N and Siakavellas NJ. Programmable thermal emissivity structures based on bioinspired self-shape materials. *Sci Rep* 2015; 5: 17682.
- Athanasopoulos N and Siakavellas NJ. Self-shape structures with programmable thermal radiative properties. In: *Multifunctional materials & structures*, Gordon Research, CA, USA, 2016.
- Gladman S, Matsumoto A, Nuzzo EA, et al. Biomimetic 4D printing. *Nat Mater* 2016; 15: 413–418.
- Czernik S. *Design of the thermal control system for compass-1*. Thesis, University of Applied Sciences Aachen, Germany, 2004.
- Scholz A, König F, Fröhlich S, et al. Flight results of the COMPASS-1 mission. *Acta Astronaut* 2010; 67: 1289–1298.
- Scholz A. COMPASS-1 concept study report, 2003.
- Beukelaers V. *From mission analysis to space flight simulation of the OUFTI-1 nanosatellite*. Thesis, University of Liège, Belgium, 2009.
- Jacques L. *Thermal design of the Oufiti-1 nanosatellite*. Thesis, University of Liège, Belgium, 2009.
- EPFL Swiss Cube, <http://swisscube.epfl.ch/> (accessed 2012).
- Ampatzoglou A, Baltopoulos A, Kotzakolios A, et al. Design and analysis of a full composite structure for the 1st Greek CubeSat by the University of Patras (UPSAT). In: *61st international astronaut congress (IAC)*, Prague, 2010.
- Ampatzoglou A, Baltopoulos A, Kotzakolios A, et al. Re-design, analysis, manufacturing and testing of a full composite structure for the 1st Greek CubeSat by the University of Patras (UPSAT). In: *4th European CubeSat symposium*, Brussels, Belgium, 2012.
- Delfi Space. <http://www.delfispace.nl/delfi-c3/structure-mechanisms-thermal-control> (accessed 2008).
- Bulut M and Sozbir N. Analytical investigation of a nanosatellite panel surface temperatures for different

altitudes and panel combinations. *Appl Therm Eng* 2015; 75: 1076–1083.

40. Bulut M, Kahriman A and Sozbir N. Design and analysis for thermal control system of nanosatellite. In: *Proceedings of the ASME 2010 international mechanical engineering congress & exposition*, Vancouver, Canada, 2010.
41. Corpino SM, Caldera F, Nichele M, et al. Thermal design and analysis of a nanosatellite in low earth orbit. *Acta Astronaut* 2015; 115: 247–261.
42. Dahlquist G and Bjorck A. *Numerical methods*. New York: Dover Publications, 1974, pp.227–233.
43. Hemmer JH. Solar absorptance and thermal emittance of some common spacecraft thermal-control coatings. NASA Reference Publication 1121, Goddard Space Flight Center, USA, 1984.

Appendix

Notation

$a_{S_s}(T)$	solar absorptivity	I_S	solar flux
$a_{S_b}(T)$	absorptivity of the albedo	T_0	temperature at the middle of the effective emissivity curve
$a_{IR}(T)$	absorptivity from the Earth	T_{\max}	worst hot case
A	overall area of each side of the nanosatellite	T_{\min}	worst cold case
A_{Mat1}	area of the solar cells	$\alpha_{\min}, \alpha_{\max}$	minimum maximum effective absorptivity
A_{Mat2}	area of the smart surface or of a coating with constant thermo-optical properties	ΔT	difference of the minimum calculated temperature of the worst cold case the maximum temperature of the worst hot case
		ΔT_{smart}	temperature span of the effective emissivity curve
		$\epsilon_{\min}, \epsilon_{\max}$	minimum maximum effective emissivity
		$\epsilon_{\text{side}}(T), \alpha_{\text{side}}(T)$	equivalent emissivity absorptivity of each side
		$\epsilon_{Mat1}, a_{Mat1}$	emissivity the absorptivity of solar cells
		$\epsilon_{Mat2}(T), a_{Mat2}(T)$	effective emissivity absorptivity of the smart surfaces
		$\epsilon'_{IR}(T)$	emissivity of the sides of the satellite that reject heat into deep space
		$\epsilon_{IR}(T)$	IR emissivity of the Earth-oriented side

Appendix I

Detailed results from the different design scenarios

Tables 6 and 7 summarize the values of the thermo-optical properties of the different materials and

the equivalent thermo-optical properties of the sides of the Cubesat for the design scenario B and design scenario C.

Table 6. Material properties of the various studied cases; the smart surfaces cover 30% of the each side (sides 1, 2, 3, 5, 6) and 100% of side 4.

Solar cells		Smart materials' coatings		Equivalent properties of the sides							
		Internal coating ^{30,43}	External coating ^{28,43}	Sides with solar cells (1, 2, 3, 6) – 70% Sc + 30% smart surface		mpty side (4) – 100% smart surface		Bottom side (5) – 70% Sc + 30% smart surface			
				Black	Aluminum	Min	Max	Min	Max	Max	Min
Case 1		ϵ	0.85	0.900	0.080	0.621	0.865	0.088	0.900	0.865	0.621
		α	0.92	0.970	0.365	0.755	0.935	0.354	0.970	0.935	0.755
Case 2		Martin black velvet paint		Silver	Min	Max	Min	Max	Max	Min	
		ϵ	0.85	0.940	0.020	0.603	0.874	0.029	0.93	0.874	0.604
		α	0.92	0.910	0.040	0.658	0.917	0.039	0.91	0.917	0.659
Case 3		White (white zinc oxide)		Aluminum polished	Min	Max	Min	Max	Max	Min	
		ϵ	0.85	0.930	0.030	0.606	0.874	0.039	0.930	0.874	0.607
		α	0.92	0.160	0.090	0.671	0.692	0.087	0.160	0.692	0.671

Table 7. Material properties of the various studied cases; the smart surfaces cover 100% of the each side (sides 1, 2, 3, 4, 6).

Solar cells		Smart materials' coatings		Equivalent properties of the sides							
		Internal material ^{30,43}	External material ^{30,43}	100% smart surface over the solar cells (1, 2, 3, 6)		Empty side (4) (100% smart surface)		Bottom side (5) (70% Sc + 30% Al polished)			
				Black	Aluminum	Min	Max	Min	Max	Min	Max
Case 1		ϵ	0.85	0.900	0.080	0.088	0.773	0.088	0.900	0.865	0.865
		α	0.92	0.970	0.365	0.371	0.864	0.371	0.970	0.935	0.935
Case 2		Martin black velvet paint		Silver	Min	Max	Min	Max	Min	Max	
		ϵ	0.85	0.940	0.020	0.028	0.767	0.029	0.930	0.874	0.874
		α	0.92	0.910	0.040	0.049	0.832	0.048	0.910	0.917	0.917
Case 3		White (white zinc oxide)		Aluminum polished	Min	Max	Min	Max	Min	Max	
		ϵ	0.85	0.930	0.030	0.038	0.768	0.039	0.930	0.874	0.874
		α	0.92	0.160	0.090	0.098	0.837	0.091	0.160	0.692	0.692